Process Safety and Environmental Protection 192 (2024) 401–411

Contents lists available at ScienceDirect

Process Safety and Environmental Protection

journal homepage: www.journals.elsevier.com/process-safety-and-environmental-protection

Thin film nanocomposite membranes based on renewable polymer Pebax® and zeolitic imidazolate frameworks for CO_2/CH_4 separation

Dalia Refaat [a,b], Mohamed Yahia [a,b,c], Joaquín Coronas [a,b,*]

[a] Instituto de Nanociencia y Materiales de Aragón (INMA), CSIC-Universidad de Zaragoza, Zaragoza 50018, Spain
[b] Chemical and Environmental Engineering Department, Universidad de Zaragoza, Zaragoza 50018, Spain
[c] Chemistry Department, Faculty of Science, Helwan University, Cairo 11795, Egypt

ARTICLE INFO

Keywords:
Zeolitic imidazolate framework (ZIF)
Pebax® Rnew® 30R51
CO_2/CH_4 separation
Thin film composite (TFC) membrane
Thin film nanocomposite (TFN) membrane

ABSTRACT

This study investigates the impact of integrating Pebax® Rnew® 30R51, a sustainable elastomer-type copolymer material, with zeolitic imidazolate frameworks (ZIFs) to develop advanced membranes for CO_2/CH_4 gas separation. The fabrication process of ZIF/Pebax® Rnew® 30R51 thin films was optimized to achieve uniform and defect-free thin film composite (TFC) membranes. Crucial membrane properties, including permeability, selectivity and separation efficiency, were analyzed with variations in ZIF type, loading levels, film thickness and operating conditions. Additionally, the resulting TFC and ZIF/Pebax® Rnew® 30R51 thin film nanocomposite (TFN) membranes were subjected to characterization via FTIR, XRD, TGA and SEM to evaluate their physicochemical properties. Nanoparticles of ZIF-8, NH_2-ZIF-8 and ZIF-94 were individually added (at 5–15 wt% loadings) to the Pebax® Rnew® 30R51 matrix to develop the CO_2 separation efficiency. The pristine TFC membrane showed a 66 GPU CO_2 permeance and a 37.5 CO_2/CH_4 separation selectivity, primarily due to improved CO_2 mass transport. Upon inclusion of ZIFs, the CO_2 permeance with 5 wt% loadings of ZIF-8, NH_2-ZIF-8 and ZIF-94 increased to 148, 99 and 125 GPU, respectively, despite this, the CO_2/CH_4 separation selectivity maintained at 29.4, 37.0 and 27.0, respectively.

1. Introduction

Earth's climate is being influenced by greenhouse gases such as carbon dioxide (CO_2) and methane (CH_4), which trap heat in the atmosphere and raise global temperatures. (Kárászová et al., 2020; Saini and Awasthi, 2022; Zhang et al., 2013) Carbon dioxide is a major concern due to its abundance in industrial emissions, primarily from the burning of fossil fuels (Kárászová et al., 2020; Saini and Awasthi, 2022; Zhang et al., 2013).Despite being in smaller amounts, CH_4 is a strong greenhouse gas that has a greater capacity to trap heat than CO_2 over shorter periods of time (Freeman, 1999; Robeson, 1991). Therefore, for CO_2 and CH_4 to have as little of an environmental impact as possible, they must be separated effectively. One area of significant research and development is the advancement of gas separation technologies specifically designed for CO_2/CH_4 separation (Kárászová et al., 2020; Saini and Awasthi, 2022; Zhang et al., 2013). Various methods are being explored, with a notable emphasis on polymeric membrane technology. Polymeric membranes offer advantages such as cost-effectiveness, ease of scalability and energy efficiency (Kárászová et al., 2020; Saini and Awasthi, 2022; Zhang et al., 2013). In gas separation processes, membranes selectively allow certain gases to pass through while blocking others based on differences in their molecular sizes or interactions with the membrane material (Baker and Low, 2014; Basu et al., 2010; Dong et al., 2013; Wang et al., 2016; Yu et al., 2024; Zou and Zhu, 2018). The development of specialized polymeric membranes for CO_2/CH_4 separation involves engineering materials that exhibit high permeability and selectivity (Baker and Low, 2014; Basu et al., 2010; Dong et al., 2013; Wang et al., 2016; Yu et al., 2024; Zou and Zhu, 2018). Researchers are exploring membranes that can efficiently and selectively separate CO_2 from gas mixtures, allowing for the generation of cleaner and more environmentally friendly streams. The application of advanced materials and membrane technologies in CO_2/CH_4 gas separation not only contributes to environmental sustainability by reducing greenhouse gas emissions but also holds potential for various industrial applications, including carbon capture and utilization, natural gas purification and biogas upgrading (Baker and Low, 2014; Basu et al., 2010; Dong et al., 2013; Wang et al., 2016; Yu et al., 2024; Zou and Zhu, 2018).

While membrane separation is an appealing technology, it does have

* Corresponding author at: Instituto de Nanociencia y Materiales de Aragón (INMA), CSIC-Universidad de Zaragoza, Zaragoza 50018, Spain.
E-mail address: coronas@unizar.es (J. Coronas).

https://doi.org/10.1016/j.psep.2024.10.053
Received 22 August 2024; Received in revised form 1 October 2024; Accepted 15 October 2024
Available online 18 October 2024

its limitations, particularly in gas separation applications (Baker and Low, 2014; Yu et al., 2024). The primary challenge, as highlighted by Robeson in 1991 (Robeson, 1991) and 2008, (Robeson, 2008) is to overpass the intrinsic balance between permeability and selectivity regarding polymeric membranes. Typically, selectivity is low in polymers with high permeability and vice versa (Robeson, 1991, 2008). To tackle this problem, flexible polymers like polyether (PE) can be blended with strong ones like polyamide (PA), polyimides (PI) and polystyrene (PS) (Dai et al., 2016).

Pebax® Rnew® 30R51, an elastomeric poly(ether-block-amide) copolymer, emerges as a promising material for gas separation applications due to its unique segmented structure. It consists of polyamide (PA) blocks that provide mechanical strength, and polyethylene oxide (PEO) segments that enhance gas permeability, particularly for CO_2. Compared to the commonly used Pebax® 1657, Pebax® Rnew® 30R51 contains a higher polyether content, which is expected to result in superior gas permeability and more effective polymer-filler interactions when combined with ZIFs nanoparticles (Martínez-Izquierdo et al., 2022b; Murali et al., 2023a; Wang et al., 2022). These interactions are estimated to improve the dispersion and compatibility of the ZIF fillers within the polymer matrix, leading to enhanced separation performance. Moreover, Pebax® Rnew® 30R51 is derived from renewable castor oil, making it a more sustainable alternative to the fossil-based Pebax® 1657 (Martínez-Izquierdo et al., 2022b; Murali et al., 2023a; Wang et al., 2022). The use of bio-based raw materials not only reduces the carbon footprint but also aligns with eco-friendly manufacturing practices, addressing the growing demand for sustainable membrane materials. Therefore, integrating Pebax® Rnew® 30R51 with MOFs in gas separation membranes could potentially outperform the traditional Pebax®1657 membrane composites, offering both enhanced gas separation efficiency and environmental benefits (Luo et al., 2024; Martínez-Izquierdo et al., 2022b; Murali et al., 2023a; Wang et al., 2022).

The potential of metal-organic frameworks (MOFs), a subgroup known as zeolitic imidazolate frameworks (ZIFs), in gas separation has been intensively investigated, particularly when utilized as continuous polycrystalline membranes or in MMMs (Berned-Samatán et al., 2023; Jomekian et al., 2016; Liu et al., 2014; Martínez-Izquierdo et al., 2022b; Yahia et al., 2024, 2021). Among these, ZIF-8 (Park et al., 2006) and ZIF-94 (Morris et al., 2012) (also known as SIM-1 (Aguado et al., 2010)), both with the SOD type structure, stand out as ones of the most extensively studied members (Berned-Samatán et al., 2023; Jomekian et al., 2016; Liu et al., 2014; Martínez-Izquierdo et al., 2022b; Yahia et al., 2024, 2021). Their narrow microporosity and CO_2-philicity (enhanced in the case of ZIF-94/SIM-1 due to the carboxyaldehyde group of its linker) makes them promising candidates for CO_2 separation in MMMs, garnering significant attention in this field.

The interaction between the ZIF fillers and polymers (in particular, Pebax® Rnew® 30R51) matrix is crucial for optimizing membrane performance. ZIF nanoparticles introduce additional CO_2-philic sites within the polymer matrix, promoting selective sorption and diffusion of CO_2 molecules. Each ZIF variant interacts uniquely with the polymer due to its distinct functional groups and surface chemistries (Martínez-Izquierdo et al., 2022b; Wang et al., 2022). ZIF-8, with its basic framework, enhances CO_2 permeability but offers moderate selectivity due to its neutral surface. NH_2-ZIF-8, incorporating amino groups, establishes specific hydrogen bonding interactions with CO_2 molecules, thereby improving CO_2/CH_4 selectivity compared to ZIF-8. ZIF-94, known for its hydrophilic properties, further increases CO_2 affinity and contributes to higher selectivity, while the SALE (solvent-assisted ligand exchange) modification fine-tunes these interactions by adjusting the ligand environment to optimize diffusion pathways (Madhav et al., 2020; Morris et al., 2012; Park et al., 2006). The incorporation of these ZIFs at various loadings demonstrates a significant enhancement in CO_2 permeance and selectivity, indicating the effectiveness of tailored filler-polymer interactions in developing advanced membranes for efficient gas separation.

The novelty of the current study lies in demonstrating the feasibility of synthesizing and integrating distinct ZIFs (ZIF-8, NH_2-ZIF-8 and ZIF-94) into a sustainable polymer matrix, Pebax® Rnew® 30R51. This polymer derives from renewable plant resources, significantly reducing dependence on fossil-based resources while lowering the carbon footprint and contributing to a more sustainable lifecycle. Therefore, the integrating of Zn-based MOFs into the bio-based matrix not only promotes the development of greener membrane technologies, but also leverages the unique advantages of each ZIF, such as their specific pore sizes and functional properties.

ZIF-8, with a pore size of approximately 0.34 nm, effectively facilitates CO_2 separation from methane primarily through two mechanisms. First, the pore size is ideal for size exclusion, allowing the smaller CO_2 molecules (kinetic diameter ~0.33 nm) to pass through while partially excluding the larger CH_4 molecules (kinetic diameter ~0.38 nm). Second, ZIF-8 exhibits selective adsorption due to its nitrogen-rich framework, which has a higher affinity for CO_2 than for CH_4. Together, these mechanisms make ZIF-8 highly effective in separating CO_2 from CH_4 gas (Madhav et al., 2020; Morris et al., 2012; Park et al., 2006; Tanvidkar et al., 2022), The pore size of ZIF-8 (0.34 nm) is generally stable during the selectivity test, allowing CO_2 (kinetic diameter 0.33 nm) to pass more readily than CH_4 (0.38 nm). However, ZIF-8 may exhibit the phenomenon called "gate opening", where the framework undergoes slight flexibility under specific conditions, such as gas adsorption or pressure changes. This flexibility can temporarily increase the pore size slightly (Fairen-Jimenez et al., 2011). Despite this, the selective behavior of ZIF-8 remains largely intact during CO_2/CH_4 separation due to its inherent preference for CO_2 adsorption.

NH_2-ZIF-8 retains a similar pore structure but incorporates functional amino groups, and ZIF-94 and its SALE variant feature slightly larger, tunable pore sizes around 0.38 nm (Madhav et al., 2020; Morris et al., 2012; Park et al., 2006). The precise control over the pore size and chemistry of these ZIFs enables tailored interactions with CO_2 molecules, significantly enhancing both CO_2 permeability and CO_2/CH_4 selectivity. This innovative approach emphasizes the potential of ZIF-incorporated Pebax membranes to achieve superior gas separation performance, addressing critical environmental and energy challenges.

Therefore, the spin-coating method was employed to fabricate polymer Pebax® Rnew® 30R51 thin-film composite (TFC) membranes on porous polysulfone (PSF) supports. While spin-coating is effective for laboratory-scale membrane production, we acknowledge that alternative fabrication techniques, such as dip-coating, interfacial polymerization, or roll-to-roll processes, would be more suitable for large-scale industrial applications. These methods are widely recognized for scaling up membrane fabrication while maintaining the thin active layer needed for optimal performance (Alkandari and Castro-Dominguez, 2024). Our work contributes valuable insights into the academic knowledge base by demonstrating the performance of Pebax® Rnew® 30R51-based thin-film nanocomposite (TFN) membranes, particularly those incorporating MOFs like ZIF-8 and ZIF-94, under realistic mixed gas conditions.

In this work, various TFC membranes were prepared by adjusting the polymer solution concentration (0.25–5 wt%), with the optimal condition used to create thin-film nanocomposite (TFN) membranes by incorporating different loadings (5–15 wt%) of ZIFs ZIF-8, NH_2-ZIF-8 and ZIF-94. Physicochemical characterization demonstrated that the inclusion of ZIFs in the Pebax® Rnew® 30R51 matrix enhanced CO_2/CH_4 separation performance. Pebax® Rnew® 30R51 is relatively new to gas separation applications, with limited research on its combination with MOFs (Martínez-Izquierdo et al., 2022b). In fact, this last work devoted to ionic liquid membranes with MOF ZIF-94.

2. Experimental

2.1. Materials

Solvay Advanced Polymers supplied the polysulfone (Udel® P-3500 LCD). Zinc nitrate hexahydrate ($Zn(NO_3)_2{\cdot}6\,H_2O$) and methyl imidazole (mIm) were bought from Sigma Aldrich, Spain. 2-aminobenzimidazole (2-ambzIm, 97 %) were bought from Sigma Aldrich, Spain. Acros Chemicals in Spain supplied 4-methyl-5-imidazole-carboxyaldehyde (camIm). From Fluorchem in the UK, we acquired poly[1-(trimethylsilyl)prop-1-yne] (PTMSP). Arkema, France, kindly supplied polyether-block-amide, Pebax® Rnew® 30R51 in pellet form. This thermoplastic elastomer consists of flexible polyether and rigid polyamide components, sourced from renewable materials (41 % renewable carbon). The following solvents were purchased in that order from Análisis Vínicos, Panreac, Labbox, and Scharlab, Spain: methanol (MeOH) and isopropanol, N-methyl-2-pyrrolidone (NMP), 1-propanol (1-PrOH) and 1-butanol (1-ButOH). The gases used in the separation tests were provided by Abelló Linde S.A., Spain. All the solvents, gasses and polymers were used without additional purification.

2.2. Methods

2.2.1. Synthesis of asymmetric PSF supports

Phase inversion methodology was used to construct PSF supports as previously reported (Martínez-Izquierdo et al., 2022b). Initially, a dope solution consisting of 20 wt% PSF in NMP was prepared by stirring at room temperature (RT) overnight. Using an Elcometer 4340 automatic film applicator, the PSF supports were deposited onto a Teflon plate, achieving a 250 μm thickness after the polymer solution had been poured and degassed. The casting speed was 0.04 m s^{-1}. Subsequently, the freshly cast membranes underwent a phase inversion process by immersion in a water bath at RT for 1 h. The membranes were rinsed and cleaned with isopropanol after being completely precipitated and immersed in a deionized (DI) water bath overnight, afterward the PSF supports were dried inside a vacuum oven at 100 °C overnight.

2.2.2. Synthesis of ZIF-8

ZIF-8 nanoparticles (ca. 30 nm in size) were synthesized following slightly altering a previously published method (Martínez-Izquierdo et al., 2022b). In a typical procedure, 1.467 g of $Zn(NO_3)_2{\cdot}6\,H_2O$ (4.93 mmol) and 3.245 g of ligand 2-methylimidazole (mIm, 39.52 mmol) were separately dissolved in 150 mL of methanol (MeOH). The ligand solution was subsequently added into the metal solution while stirring. The mixture obtained was stirred at RT for 30 min, followed by centrifugation at 9000 rpm for 10 min and four rinsing steps with MeOH. After that, the resultant product was dried and activated for an entire night at 40°C.

2.2.3. Synthesis of NH_2-ZIF-8

NH_2-ZIF-8 nanoparticles (ca. 33 nm in size) were synthesized following a previously reported method (Thompson et al., 2013). A solution was prepared by dissolving 2-ambzIm (0.549 g, 4 mmol) and mIm (1.340 g, 16 mmol) in MeOH (50 mL). After 2 h of vigorous stirring at 50 °C, the mixed-linker solution turned transparent. Simultaneously, Zn $(NO_3)_2{\cdot}6\,H_2O$ (2.5 mmol) was dissolved in MeOH (50 mL). Upon cooling the mixed-linker solution to 23 ± 2 °C, the mixture was stirred for 1.5 h after adding the Zn salt solution, resulting in a milky suspension. After being centrifuged at 2500 rpm for 30 min, the product was washed three times with fresh MeOH, then vacuum-dried at 80 °C for 12 h, with an extra drying step for one hour at 150 °C.

2.2.4. Synthesis of ZIF-94 by solvent-assisted ligand exchange (SALE)

ZIF-94(SALE) nanoparticles (ca. 48 nm in size) were synthesized following a previously reported method (Martínez-Izquierdo et al., 2022b). Initially, 0.323 g of ca. mIm (2.94 mmol) was dissolved in 20 mL of 1-ButOH. Subsequently, after adding 100 mg of nano ZIF-8, the mixture was stirred at room temperature for 24 h. After centrifugation was used for 10 min at 9000 rpm to extract the final product, the crystals underwent four separate washings with fresh 1-butanol under the same parameters. The final crystals were then allowed to dry at 40°C for the entire night.

2.2.5. Synthesis of ZIF-94

ZIF-94 (ca. 180 nm in size) was produced using a previously established protocol based on the reuse of the crystallization mother liquor (Hasan et al., 2022). In brief, following the ZIF-94 synthesis, the mother liquor was isolated from the nanocrystals via centrifugation for re-use in a subsequent synthesis of ZIF-94.

2.2.6. Membrane preparation

The TFC and TFN membranes were prepared following the previous reported studies (Martínez-Izquierdo et al., 2022b). A PTMSP gutter layer was applied by spin-coating onto the PSF supports to prevent the selective layer from penetrating. Initially, a 2 wt% PTMSP solution was obtained by dissolving the polymer in n-hexane at RT. The support, securely attached to the spin coater (Model WS-650MZ-23NPP/A1/AR1) was coated with the solution (0.7 mL) spinning at 2500 rpm for 20 s. Following that, the supports, now with the gutter layer, were heated in an oven at 40 °C for 1 h to eliminate any remaining solvent through evaporation. The ultimate selective layer was applied by spin-coating onto the PTMSP/PSF supports at 2500 rpm for 20 s. To achieve this, a solution of Pebax® Rnew® 30R51 was prepared by dissolving 0.2 g of the polymer in a 1-PrOH/1-ButOH (3/1 v/v) mixture (9.8 g) under reflux at 80 °C for 2 h. To prevent gelation, the polymer solution was submerged in a water bath at 45°C. Finally, this solution (0.6 mL) was applied onto the PTMSP/PSF support and spun (2500 rpm, 20 s) to create the Pebax® Rnew® 30R51 /PTMSP/PSF membranes, designated as TFC membranes.

Following the evaluation of TFC membranes in the gas separation setup, the ideal condition was identified for fabricating TFN membranes incorporating ZIF nanocrystals. Under these conditions, the polymer was dissolved in 2/3 of the total solvent, maintaining the same parameters. Simultaneously, varying amounts of ZIF particles (ranging from 5 to 15 wt% relative to the MMM) were dispersed in the remaining solvent (1/3 of the total) using an ultrasonic bath. After dissolving the polymer and cooling it to 40–45 °C, the ZIF suspension was introduced into the solution and stirred. The suspensions containing ZIFs were stirred at 45 °C for 1 h before spinning. The resulting membranes were designated as TFN/ZIF-8(Y), TFN/NH_2-ZIF-8(Y), TFN/ZIF-94(SALE)(Y) and TFN/ZIF-94(Y), where Y represents the MOF loading (wt%). After the spinning process, all membranes were treated at 40 °C for 18 h to allow for the thorough removal of any residual solvent.

2.3. Characterization of ZIFs and membranes

Images of both ZIF powders and membranes were captured using a scanning electron microscope (Inspect F50 model by FEI) operating at 10 kV. Furthermore, the instrument was utilized to determine the thickness of the selective skin layer at 5–6 various positions along the membrane. For the preparation of membrane cross-sections, after immersion in liquid nitrogen, the samples were freeze-fractured and subsequently coated with Pd. Thermogravimetric analyses (TGA) was performed with Mettler Toledo TGA/STDA 851e instrument. Approximately 3 mg of ZIF powder was meticulously loaded into 70 mL alumina pans. Subsequently, the samples underwent controlled heating, gradually increasing from 35 to 700 °C at a rate of 10 °C min^{-1}, all while maintaining an airflow of 40 cm^3 (STP) min^{-1}. The Bruker Vertex 70 FTIR spectrometer, which has a Golden Gate diamond ATR attachment and a DTGS detector, was used for FTIR analysis. Averaging 60 scans over the wavenumber range of 4000–600 cm^{-1}, spectra were produced with a resolution of 4 cm^{-1}. The crystallinity of the samples was analyzed using Panalytical Empyrean equipment with CuKα radiation (λ =

0.154 nm) through X-ray diffraction (XRD). The assessment spanned from 5° to 40° with a scan rate of 0.03° s^{-1}.

The elemental analysis was performed via a Perkin Elmer Series II 2400 CHNS/O Analyzer, employing the CHNS method without extra oxygen flow to boost combustion, the samples, placed in tin capsules, were weighed by a Provectus 6500 microbalance at room temperature.

2.4. Gas separation tests

The 2.12 cm^2 membrane samples were positioned within a module comprising two stainless steel components and a 316LSS macro-porous disk support (Mott Co., featuring a 20 µm nominal pore size), securely hold in place with Viton O-rings. The temperature (within the 25–50 °C range) was regulated by placing the permeation module inside a UNE 200 Memmert oven. Gas separation measurements were conducted by introducing the CO_2/CH_4 mixture (50/50 cm^3 (STP) min^{-1} with Alicat Scientific MC-100CCM-D mass flow controllers) to the feed side at an operating pressure of 3 bar. The permeate side of the membrane was swept with 4.5 cm^3(STP) min^{-1} of He at atmospheric pressure (about 1 bar) using an Alicat Scientific MC-5CCM-D controller. The stage cut (θ), defined as the ratio of permeate to feed flow rate, was approximately 2 %. Concentrations of CO_2 and CH_4 in the permeate side were analyzed online using an Agilent 3000 A micro-gas chromatograph. Permeances of CO_2 and CH_4 were calculated in GPU (gas permeance unit, 10^{-6} cm^3 (STP) cm^{-2} s^{-1} $cmHg^{-1}$) once steady state in the exit stream was achieved. The CO_2/CH_4 separation selectivities were determined as the ratios of the corresponding permeances. The gas measurements results were performed for three different membrane samples under the same conditions, and the average values along with their corresponding errors were recorded.

3. Results

3.1. Characterization of ZIF-8, NH_2-ZIF-8, ZIF-94(SALE) and ZIF-94

ZIF-8, NH_2-ZIF-8, ZIF-94(SALE) and ZIF-94 were synthesized for application as fillers in Pebax® Rnew® 30R51 thin film nanocomposite (TFN) membranes. The ZIF-8, NH_2-ZIF-8, ZIF-94(SALE) and ZIF-94 average particle sizes are 30 ± 5 nm, 33 ± 6, 48 ± 8 nm and 180 ± 73 nm, respectively, as illustrated in Fig. 1 and Fig. S1 **(refer to** supplementary information**)**.

Thermogravimetric analyses (TGA) were conducted in an air atmosphere, covering a temperature range of 35–700 °C. The results (depicted in Fig. 2**a**) show that the ZIFs synthesized particles degrade in the 200–700 °C range, while ZIF-94(SALE) and ZIF-94 notably differ from the thermal degradation behavior of ZIF-8 and NH_2-ZIF-8 before 200 °C. The weight losses below ca. 200 ºC, more significant for the hydrophilic in nature ZIF-94 materials, correspond to remaining polar solvents. ZIF-94(SALE) and ZIF 94 nanoparticles degrade at their fastest rate between 375 and 400 °C, while ZIF-8 and NH_2-ZIF-8 degrade at a higher temperature of about 450 °C. Meanwhile, NH_2-ZIF-8 with a different ligand content is always stable before 400 °C, which consistent with the integration of ambzIm into the original ZIF-8 structure coordinated to the metal, not only trapped in its cavities (Xiong et al., 2022). Moreover, the TGA curve of ZIF-94 shows no weight loss attributed to the presence of organic ligands trapped in the pores, indicating an

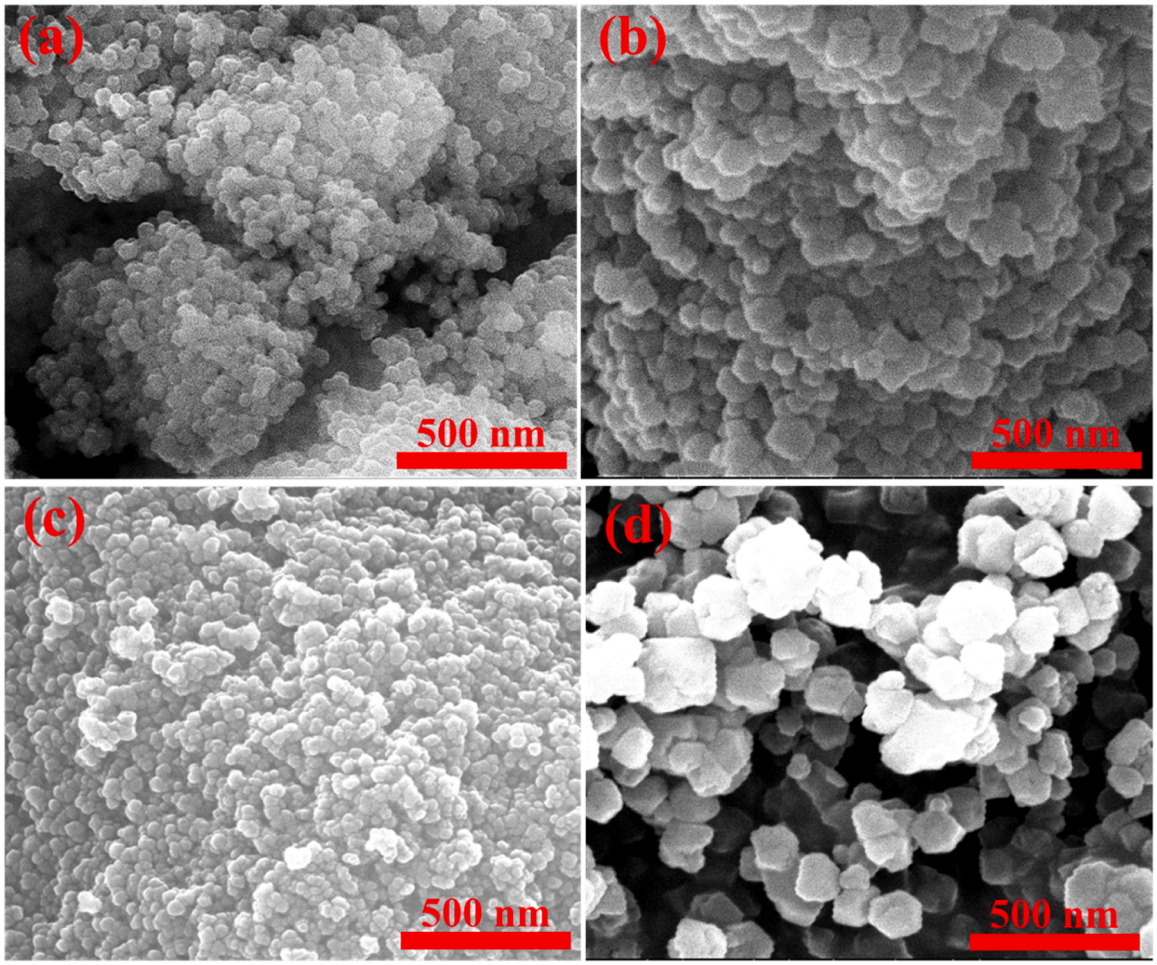

Fig. 1. SEM images for ZIF particles: ZIF-8 (a), NH_2-ZIF-8 (b), ZIF-94(SALE) (c) and ZIF-94 (d).

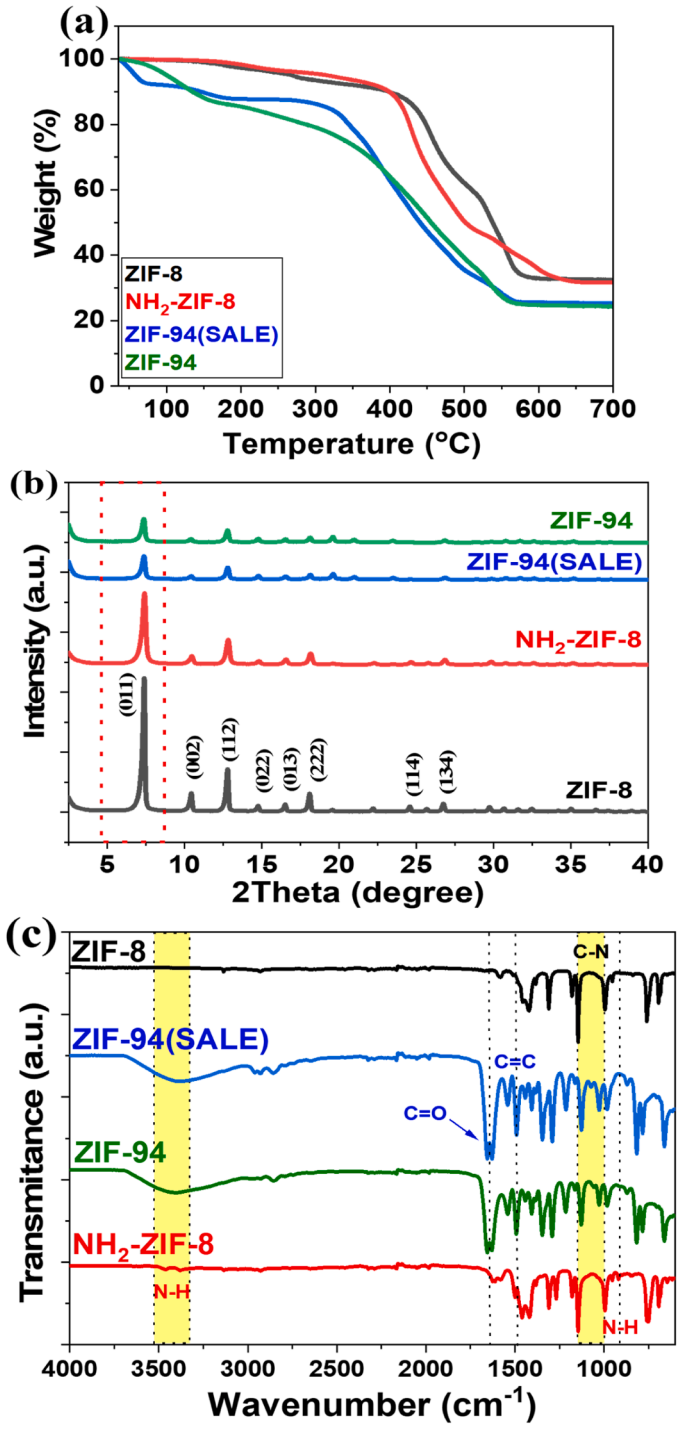

Fig. 2. ZIF powders: TGA curves (a), XRD patterns (b) and ATR-FTIR spectra (c).

effective activation of the material (Martínez-Izquierdo et al., 2022b).

The XRD analysis confirmed the crystallinity and purity of the ZIF particles, as depicted in Fig. 2**b**. This figure shows the ZIF-8 characteristic diffraction peaks, which correspond to the planes (011), (002), (112), (022), (013), (222), (114) and (134), in good agreement with earlier findings, confirming the SOD type structure of ZIF-8 (Park et al., 2006). The XRD analysis of NH_2-ZIF-8 indicates that substituting the original ligand of ZIF-8 with a primary amine imidazole ligand, i.e. mIm linker of ZIF-8 to ambzIm linker in NH_2-ZIF-8, kept the original crystal structure, in agreement with previous reports (Thompson et al., 2012; Xiong et al., 2022). Furthermore, the XRD analysis showed that the peak positions obtained for ZIF-94(SALE) match well with those of ZIF-94 and ZIF-8 and the recorded patterns can be considered the same. This indicates the successful insertion of camIm into nanosized ZIF-8 for the production of ZIF-94(SALE), as reported in previous published studies (Martínez-Izquierdo et al., 2022b). Interestingly, the produced ZIF nanocrystals (NH_2-ZIF-8 and ZIF-94(SALE)) exhibited a higher particle size (33 ± 6 and 48 ± 8 nm, respectively) (refer to Fig. 1 and Fig. S1) and lower XRD peak intensities in comparison with the original ZIF-8 nanocrystals. This might be attributed to the fact that the ligands introduced during the exchange process are bulkier than the original ones, hence steric hindrance effects may occur, potentially leading to structural defects and distortions.

Fig. 2**c** displays the FTIR-ATR spectra of ZIFs, showing similar spectra for ZIF-94(SALE) and ZIF-94. Both show distinct bands at 1660 cm^{-3} (connected to the aldehyde group (–CHO)) and 1496 cm^{-3} (linked to the C═C bond) (Kattula et al., 2015; Wang et al., 2022). Even though ZIF-94(SALE) and ZIF-8 have similar FTIR spectra, ZIF-8 important bands which correspond to the C–N bond at 1147 cm^{-1} and 993 cm^{-1} are absent, which supports a successful ligand exchange. The FTIR-ATR spectrum of NH_2-ZIF-8 exhibits novel peaks at 3470/3385 cm^{-1} and 916/848 cm−1. These peaks, indicating the existence of –NH2 and –NH groups, show that the ambzIm linker successfully replaced the mIm linker in ZIF-8 (Xiong et al., 2022).

3.2. Characterization of TFC and TFN membranes

Fig. S2 presents the cross-section SEM images for Pebax® Rnew® 30R51 TFC membranes prepared with different concentration of polymer in the casting solution (ranging from 0.25 % to 5 % wt%), offering visual insights into the morphological changes induced by varying such parameter. Furthermore, as depicted in all images in Fig. S2, a thin layer of Pebax® Rnew® 30R51 (1–4 μm) was applied onto the PSF support membrane, with a PTMSP gutter layer positioned between the support and the Pebax selective layer. This arrangement prevents the penetration of the Pebax® Rnew® 30R51 into the PSF support, which could compromise the gas separation performance by increasing the transport resistance (Kattula et al., 2015). PTMSP polymer, being a minimally selective and highly permeable material, is anticipated to have a negligible impact on the overall gas permeation resistance (Li et al., 2013). The CO_2/CH_4 selectivity of PTMSP is typically in the range of 3–4. For comparison, the self-standing Pebax® Rnew® membrane has demonstrated a CO_2/CH_4 selectivity of approximately 20 ± 2 and a CO_2 permeance of around 113 ± 3 Barrer (Murali et al., 2023b). Based on the gas separation performance results represented in Table 1, the most effective casting solution consists of a 2 wt% concentration of Pebax® Rnew® 30R51 (66 GPU of CO_2 with a CO_2/CH_4 selectivity of 37.5, discussed below), which was then applied to for further examination in the fabrication of ZIF based TFN membranes, as shown in Fig. 3. This figure depicts the SEM images corresponding to the TFN membranes embedded with ZIF particles at 5 wt% loading, indicating the PSF

Table 1
CO_2/CH_4 mixture separation performance for the PSF support and TFC membranes with different Pebax® concentrations (0.25–5 wt%) and TFC (2 wt% Pebax® Rnew® 30R51) at different temperatures (25–50 °C).

Membrane	Temperature (°C)	Permeance CO_2 (GPU)	Permeance CH_4 (GPU)	Selectivity (CO_2/CH_4)
PSF (support)	35	411± 1	122 ± 1	3.4 ± 0.2
TFC−0.25 %	35	216 ± 23	9.7 ± 1.4	22.3 ± 0.4
TFC−0.5 %	35	191 ± 22	6.7 ± 1.0	28.5 ± 1.1
TFC−1 %	35	102 ± 17	3.7 ± 0.7	30.3 ± 1.2
TFC−2 %	35	66 ± 6	1.8 ± 0.3	37.5 ± 1.5
TFC−5 %	35	54 ± 1	2.1 ± 0.1	26.4 ± 0.3
TFC−2 %	25	59 ± 12	1.7 ± 1.1	39.5 ± 1.1
TFC−2 %	50	69 ± 5	2.5 ± 0.3	28.3 ± 1.1

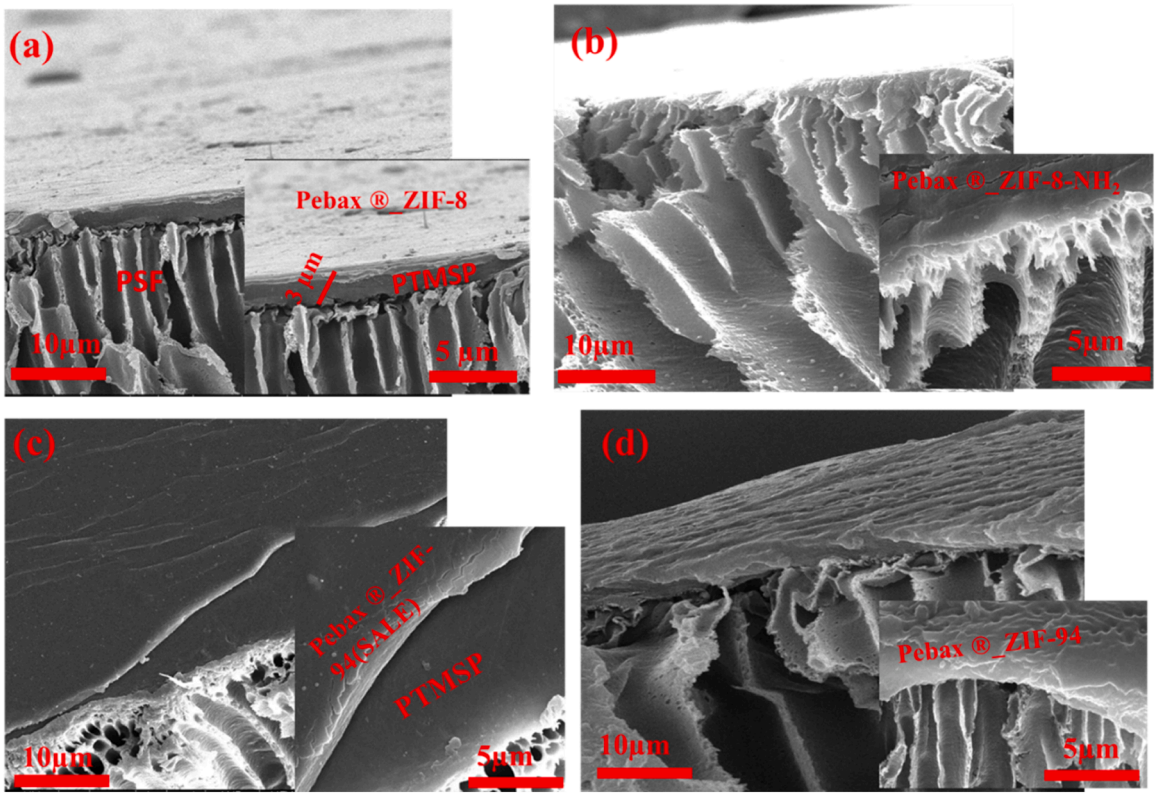

Fig. 3. SEM cross-sections for Pebax® Rnew® 30R51 TFN membranes with different ZIF nanoparticles (5 wt% loading): ZIF-8 (a), NH_2-ZIF-8 (b), ZIF-94 (SALE) (c) and ZIF-94 (d).

porous structure with Pebax® Rnew® 30R51 thin film layer and ZIF particles within the TFN membranes. As shown, the embedded ZIF particles were effectively integrated into the Pebax® Rnew® 30R51 polymer, which was coated onto the PSF support to fabricate the TFN membranes. These particles were uniformly dispersed throughout the TFN surface, with no obvious agglomeration observed on the top surface of the TFN. In any event, no apparent large MOF aggregation was observed on the top of the SEM images showing the membrane skin layer which includes the MOF particles.

Furthermore, Figs. S3 and S4 provide SEM cross-section images of TFN membranes with increased MOF loadings (10 and 15 wt%), respectively. Again, these mages indicate that there is no obvious agglomeration or accumulating of ZIF particles within the TFN membranes, similarly to the situation corresponding to the lower 5 wt% loading.

Fig. 4**a and b** represent the ATR-FTIR spectra for both TFC and TFN membranes. Even if the massive PSF signals predominate, distinctive peaks representing Pebax® and ZIFs offer insights into their successful integration. The PSF support displays distinctive peaks at 1240 cm^{-1} (aromatic C-H bending) and 1050 cm^{-1} (C-O stretch), while Pebax® Rnew® 30R51 exhibits peaks at 3370/3300 cm^{-1} (N-H stretch), 2850–2925 cm^{-1} (-CH_2- stretch), 1580 cm^{-1} (C═O stretch), and 1050 cm^{-1} (C-O stretch). Upon incorporating different ZIF particles into the TFN membranes, additional characteristic peaks appeared. For example, ZIF-8 shows peaks at 3000/2850 cm^{-1} (C-H stretch), 1635 cm^{-1} (C-N stretch) and 970 cm^{-1} (C–N bending), distinguishing it from the other ZIFs. Additionally, ZIF-94 demonstrates notable bands at 1730 cm^{-1} (aldehyde group –CHO) and 1496 cm^{-1} (C═C bond), similar to ZIF-94(SALE). Furthermore, NH_2-ZIF-8 reveals new peaks at 3370/3300 cm^{-1} (N-H stretch) and 916/848 cm^{-1} (N-H bending), indicating the presence of –NH_2 and –NH groups, respectively.

Fig. S5 depicts the XRD patterns for the TFC and TFN (at 15 wt% loading to have a clearer characterization) membrane samples, revealing a broad weak peak around (2θ ≈15–22°). This is associated to the weak crystallinity originating from the PSF support (Lu et al., 2016). Furthermore, the analysis confirmed distinct diffraction peaks corresponding to the crystalline structure of the ZIF particles (all with the SOD type structure) at 2θ values of approximately 7.3°, 10.4°and 12.9°, corresponding to the (011), (002) and (112) planes, respectively. These findings align well with the previous results (Nguyen et al., 2012; Yahia et al., 2021), confirming the successful integration of different ZIF particles into TFN membranes without apparent loss of crystallinity. Additionally, Fig. S6 illustrates the thermal stability of the TFN membranes (with 15 wt% ZIFs). As anticipated, due to the ultrathin layers deposited atop the PSF supports, the thermal stability of the membranes remained largely unchanged, which in line with the previous published studies (Martínez-Izquierdo et al., 2021; Sánchez-Laínez et al., 2018). Notably, the characteristic degradation peak of Pebax® Rnew® 30R51 at 450–500 °C is not discernible in the thermograms of the TFN membranes. However, only the degradation peaks associated with PSF at 550 °C and 650 °C are evident in the supported membranes. In summary, despite the presence of different polymers (PSF and Pebax® Rnew® 30R51) and ZIFs, the TGA curves did not provide significant insights into the incorporation of ZIF particles within the TFN membranes. This behavior can be primarily attributed to the higher proportion of PSF within the membranes in comparison with the Pebax® Rnew® 30R51 layer and ZIF nanoparticles.

Table 2 shows the elemental analysis corresponding to carbon (C), hydrogen (H), and nitrogen (N) percentages of ZIF-8-NH_2 (obtained from synthesis with the simultaneous presence of 2-methylimidazole (mIm) and 2-aminobenzimidazole (2-ambzIm)) and ZIF-94(SALE) (obtained by SALE between mIm and 4-methyl-5-imidazole-carboxyaldehyde (camIm) ligands). Also the theoretical C, H and N contents in the original ZIF-8, ZIF-8-NH_2 and ZIF-94 were calculated for comparison. The ligand exchange percentages were calculated by comparing theoretical C (%) values for scenarios with 0 % (all mIm) and 100 % (all 2-

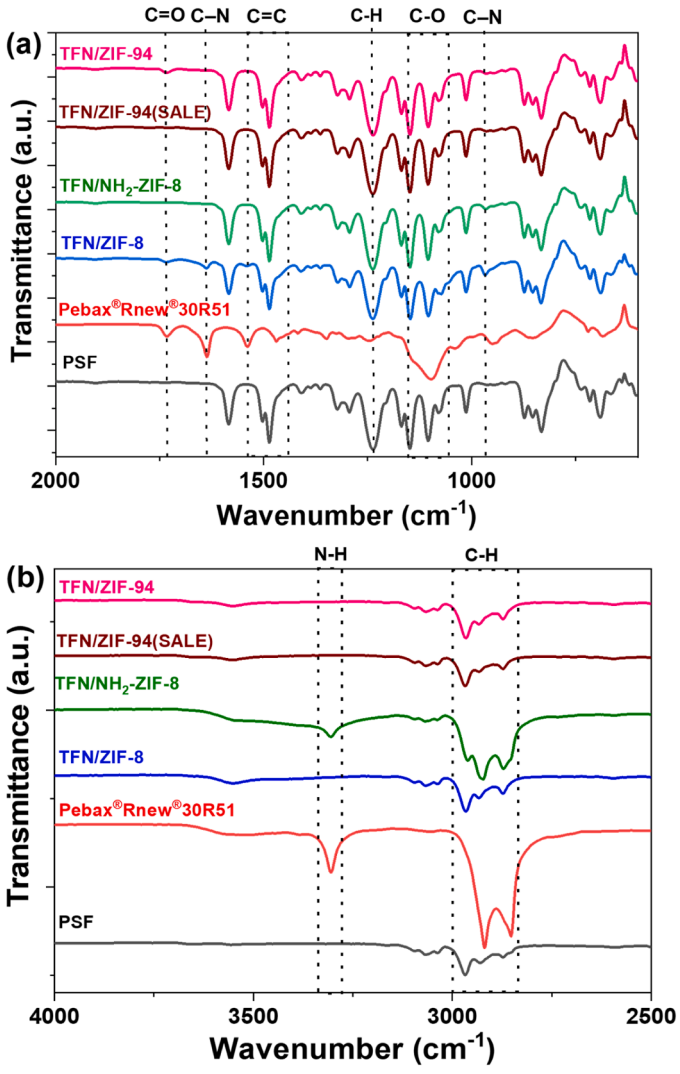

Fig. 4. ATR-FTIR spectra of PSF, Pebax® Rnew® 30R51(2 wt%) and TFN/ZIFs (15 wt%): from 2000 to 600 cm^{-1} (a) and from 4000 to 2500 cm^{-1} (b).

Table 2
The measured percentages of carbon (C), hydrogen (H), and nitrogen (N) in various samples obtained through elemental analysis, alongside theoretical calculations from ZIF formula.

ZIF	C (%)	H (%)	N (%)	Sum (%)
ZIF−8-NH_2 (Experimental)	43.3	4.4	24.3	72.1
ZIF−94(SALE) (Experimental)	41.1	4.9	16.8	62.8
ZIF−8 (Theoretical)	41.9	5.3	24.4	71.5
ZIF−8-NH_2 (Theoretical)	50.7	4.3	25.3	80.3
ZIF−94 (Theoretical)	38.3	3.9	17.9	60.1

ambzIm or camIm) ZIFs, revealing ca. 16 % 2-ambzIm in ZIF-8-NH_2 and 22 % camIm in ZIF-94. This indicates significant modifications mainly at the crystal surface due to the restricted diffusion of larger ligands within the ZIF structure.

3.3. CO_2/CH_4 separation performance

The gas separation efficiency of the TFC membranes prepared at different Pebax® Rnew® 30R51 concentration in the spin coating solution (0.25–5 wt%) was evaluated using a 50:50 CO_2/CH_4 mixture at a feed pressure of 3 bar and different temperature (25, 35 and 50 °C). A 50:50 CO_2/CH_4 mixture was used to test the selectivity in order to create a challenging separation environment and to better understand the membrane performance under high CO_2 conditions. This higher CO_2 concentration enables a clearer assessment of the membrane ability to selectively permeate CO_2 over CH_4, which is crucial for evaluating the separation mechanism in mixed matrix membranes. Although typical natural gas streams contain lower CO_2 levels (usually between 1 % and 10 %), testing with higher concentrations is common in research to stress-test the membranes and to simulate conditions encountered in scenarios like biogas upgrading, where CO_2 concentrations are much higher (40–50 %) (Biruh and Hilmi, 2012). As depicted in Table 1 and Fig. 5, when the concentration of polymer increases, the permeance of CO_2 through the TFC membranes decreases and the contrary is true for the CO_2/CH_4 separation selectivity. The increasing concentration of Pebax® Rnew® 30R51 gave rise to a thicker layer (approximately ≈ 3.5 μm ± 0.1) on top of the PSF surface where defects are minimized and thus larger CO_2/CH_4 separation selectivity is achieved. Indeed, the rise in polymer concentration enhances the CO_2/CH_4 selectivity by facilitating selective interactions between CO_2 gas molecules and the PEO (polyethylene oxide), Pebax® Rnew® 30R51 functional groups, which impart polarity to the polymer chain (Tena et al., 2015). This polarity enhances the CO_2-affinity of the TFC membranes due to the electrostatic interaction between the CO_2 quadrupole moment and the PEO sites within the Pebax® Rnew® 30R51 surface (Embaye et al., 2021; Martínez-Izquierdo et al., 2022a; Wang et al., 2015). Furthermore, the PA (polyamide) chains facilely coordinate with CO_2 molecules, thereby promoting CO_2 diffusion through the membrane, which enhances the separation of CO_2 from CH_4 (Martínez-Izquierdo et al., 2022b). However, once a certain loading (2 wt%) of Pebax® Rnew® 30R51 layer is reached, the CO_2/CH_4 selectivity starts to decline as shown with 5 wt%

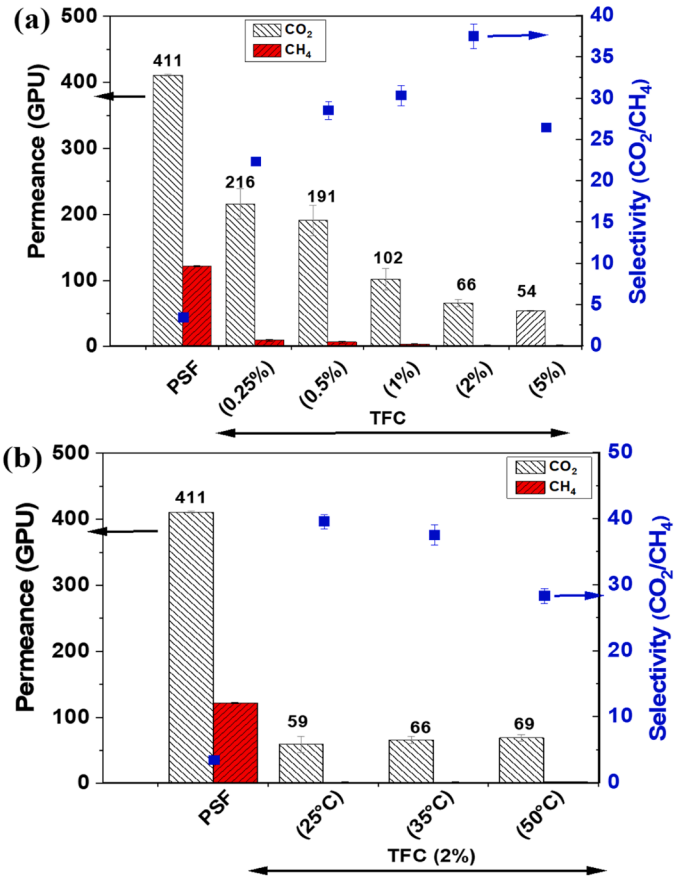

Fig. 5. Gas separation performance (CO_2/CH_4) for the fabricated TFC membranes at (a) different Pebax® Rnew® 30R51 (0.25–5 wt%) and (b) different separation temperature (25–50 °C).

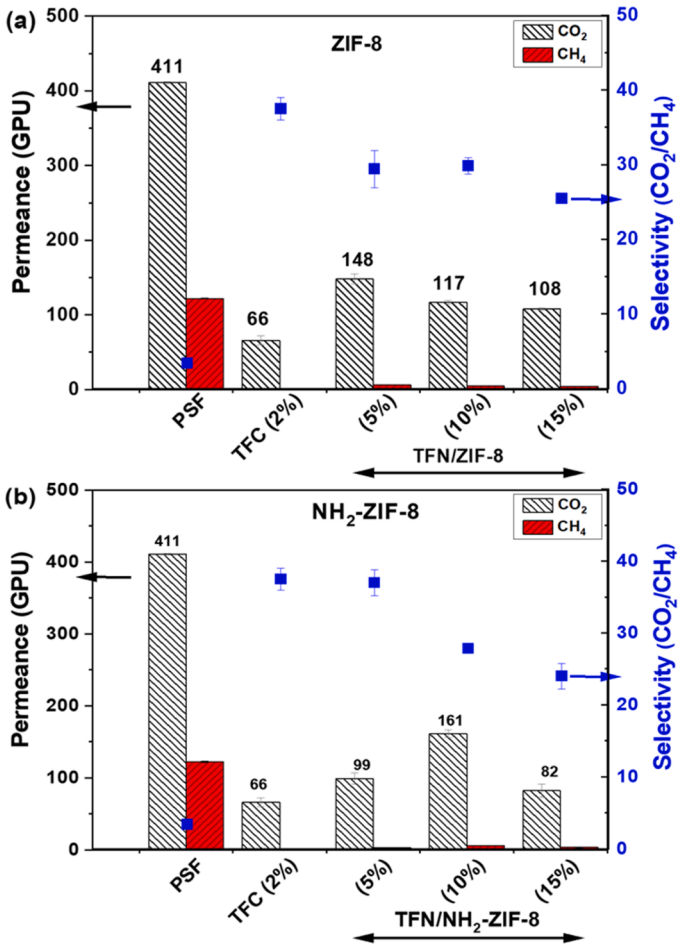

Fig. 6. Gas separation performance (CO_2/CH_4) for the fabricated Pebax® Rnew® 30R51 TFN membranes (a) TFN/ZIF-8 (5–15 wt%) and (b) TFN/NH_2-ZIF-8 (5–15 wt%).

(see Table 1 and Fig. 5). This decrease is attributed to the fact that the excessive Pebax® Rnew® 30R51 solution loading could lead to aggregation or phase separation on the PTMSP gutter layer surface by increasing the Pebax thickness, causing low CO_2 permeance and CO_2/CH_4 selectivity. Based on these results, the most effective casting solution is the one formulated with a 2 wt% of Pebax® Rnew® 30R51 and this optimal condition was applied for further investigation to prepare the ZIF/TFN membranes shown below.

Additionally, further gas separation performance was evaluated at different operating temperatures (25, 35 and 50 °C). The highest temperature (50 °C) was chosen based on previous observations of hysteresis effects on CO_2 permeability in similar membrane copolymers, which occurred around 70 °C (Martínez-Izquierdo et al., 2022a; Tena et al., 2015). This behavior may be linked to irreversible phase separation triggered by the segregation of PEO from its blend with the other copolymer (Martínez-Izquierdo et al., 2019, 2022a). Besides, the high temperatures led to a loss of separation selectivity due to a decrease of the interaction of the CO_2 molecules with the membrane materials.

Furthermore, Fig. 5**b** shows that when the temperature increases, the polymer chains become more flexible allowing gas molecules to move more freely through the membrane. This results in higher CO_2 and CH_4 permeances. However, because of this increased mobility, the membrane ability to selectively separate CO_2 from CH_4 decreases, leading to lower CO_2/CH_4 selectivity, this attributed to the interactions between the gas molecules and the membrane material weaken at higher temperatures, reducing the membrane affinity for gases, especially CO_2 (Martínez-Izquierdo et al., 2019, 2022a; Wang et al., 2022). Additionally, the CO_2/CH_4 selectivity tends to decrease as the temperature increases, primarily due to enhanced gas diffusion rates and reduced solubility selectivity at higher temperatures (Rabiee et al., 2015). As a result, the membrane becomes less effective in preferentially adsorbing CO_2, which hinders the separation process.

After studying the separation performance of the bare polymer, different MOFs (ZIF-8, NH_2-ZIF-8 and ZIF-94) were incorporated with the Pebax® Rnew® 30R51 to construct TFN membranes. The CO_2 permeances and CO_2/CH_4 selectivities of membranes TFC (2 wt%), TFN/ZIF-8 (5, 10 and 15 wt%) and TFN/NH_2-ZIF-8 (5, 10 and 15 wt%) are compared in Fig. 6 and Table 3. As expected, the incorporation of ZIF-8 and NH_2-ZIF-8 at different amounts noticeably affected the CO_2/CH_4 separation performance of TFN membranes compared to the original TFC one. In agreement with previous works (Martínez-Izquierdo et al., 2019, 2022b; Rafiul Hasan et al., 2023; Wang et al., 2022), the gradual increase in CO_2 permeance suggests that the pores within the MOFs or at their interface with the Pebax® Rnew® 30R51 matrix facilitated better selective diffusion pathways. However, increasing ZIF loading led to a significant reduction in CO_2/CH_4 selectivity after reaching 5 wt% filler loading, as notified with membranes TFN/ZIF-8 and TFN/NH_2-ZIF-8 (10 and 15 wt%), likely due to particle agglomeration within the Pebax® matrix, creating defective filler-polymer interfaces and non-uniform particle distribution within the TFN membranes (Berned-Samatán et al., 2023; Martínez-Izquierdo et al., 2022b; Rafiul Hasan et al., 2023). Moreover, the hydrophobic nature of ZIF particles and the hydrophilic nature of Pebax® Rnew® 30R51 polymer could further compromise the membrane performance by generating voids in the polymer matrix owing to the incompatibility between both ZIF fillers and the Pebax® Rnew® 30R51 polymer surface, thus reducing the separation efficiency (Berned-Samatán et al., 2023; Martínez-Izquierdo et al., 2022b; Rafiul Hasan et al., 2023; Yu et al., 2024). Additionally, by comparing membranes TFC/ZIF-8 and TFC/NH_2-ZIF-8, it is obvious that there is a decline of the CO_2 permeance with a slight enhancing in the CO_2/CH_4 separation selectivity. This could be due to specific interactions between the amino groups of NH_2-ZIF-8 and CO_2 gas molecules, favoring the separation of CO_2 over CH_4 (Hou et al., 2022; Yu et al., 2024). This selectivity enhancement compensates for the decrease in CO_2 permeance, resulting in an overall improved separation performance, reaching the highest CO_2/CH_4 selectivity at 5 wt% loading of ZIFs. Therefore, the TFN membranes fabricated with 5 wt% ZIF-8 or NH_2-ZIF-8 produced the best CO_2/CH_4 separation selectivity of 29.4 (with 148 GPU CO_2 permeance) for TFN/ZIF-8 and 37.0 (with 99 GPU CO_2 permeance) for TFN/NH2-ZIF-8.

Although the NH_2 group in ZIF-8-NH_2 enhances CO_2 affinity, the

Table 3
CO_2/CH_4 mixture separation performance at 35 °C for TFN membranes with different loadings (5–15 wt%) of ZIF-8 and NH_2-ZIF-8 fillers.

Membrane	Permeance CO_2 (GPU)	Permeance CH_4 (GPU)	Selectivity (CO_2/CH_4)
TFN/ZIF−8 (5 %)	148± 7	5.9 ± 0.2	29.4 ± 2.5
TFN/ZIF−8 (10 %)	117 ± 2	4.8 ± 0.1	29.9 ± 1.1
TFN/ZIF−8 (15 %)	108 ± 2	4.2 ± 0.1	25.5 ± 0.2
TFN/NH_2-ZIF−8 (5 %)	99 ± 8	2.7 ± 0.6	37.0 ± 1.8
TFN/NH_2-ZIF−8 (10 %)	161 ± 6	5.8 ± 0.2	27.8 ± 0.2
TFN/NH_2-ZIF−8 (15 %)	82 ± 9	3.5 ± 0.7	23.9 ± 1.8

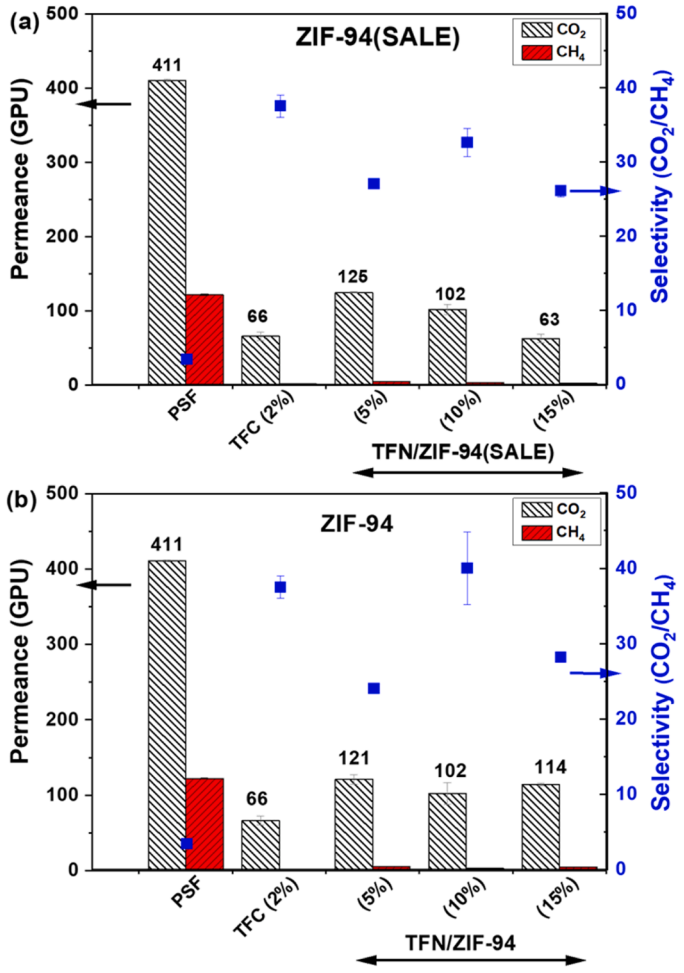

Fig. 7. Gas separation performance (CO_2/CH_4) for the fabricated Pebax® Rnew® 30R51 TFN membranes (a) TFN/ZIF-94(SALE) (5–15 wt%) and (b) TFN/ZIF-94 (5–15 wt%).

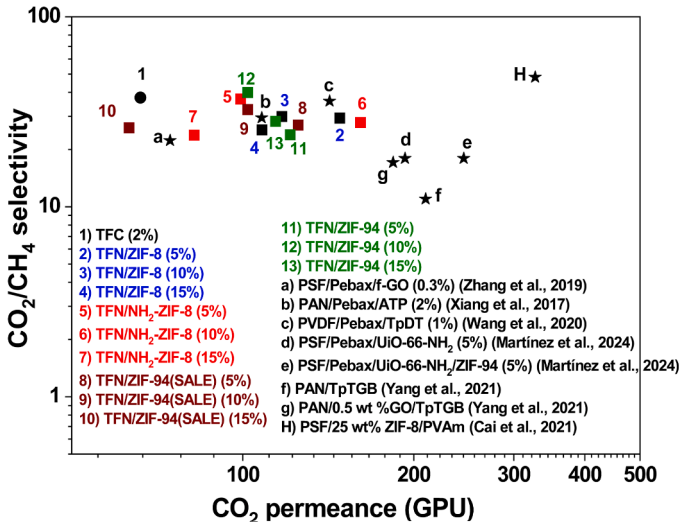

Fig. 8. CO_2/CH_4 separation selectivity as a function of CO_2 permeance at 35 °C for all the membranes in the work based on Pebax® Rnew® 30R51 in comparison with other Pebax®1657 based TFN membranes from bibliography (Cai et al., 2021; Martínez-Izquierdo et al., 2024; Wang et al., 2020; Xiang et al., 2017; Yang et al., 2021; Zhang et al., 2019), the filler loadings are in wt%.

reduced CO_2 permeance is due to stronger interactions between the NH_2 groups and the polymer matrix, which reduce free volume and restrict gas diffusion. Additionally, NH_2 groups can cause filler agglomeration, further limiting the gas transport (Xiong et al., 2022).

Moreover, the CO_2 permeance and CO_2/CH_4 selectivity values of membranes TFC (2 %), TFN/ZIF-94(SALE) (5, 10 and 15 wt%) and TFN/ZIF-94 (5, 10 and 15 wt%) are depicted in Fig. 7 and Table 4. As expected, a similar behavior like that of previous TFN membranes was observed when compared with membrane TFC (2 wt%). There is a gradually increasing in CO_2 permeance with higher loading of MOF, suggesting again that the pores within the filler enabled better selective diffusion pathways (Martínez-Izquierdo et al., 2022b; Rafiul Hasan et al., 2023; Yahia et al., 2024). However, increasing MOF loading caused a reduction in CO_2/CH_4 selectivity after reaching 10 wt% filler loading for both ZIF-94(SALE) and ZIF-94. It is worth notifying that both MOFs ZIF-94 and ZIF-8 belong to the family of zeolitic imidazolate frameworks, sharing the same SOD type structure. However, they differ by utilizing the organic linker (imidazolate carboxy-aldehyde), resulting in a hydrophilic nature for ZIF-94 compared to ZIF-8 (Gupta et al., 2016).

It is predicted that the exchange of ZIF-8 (hydrophobic MOF) with ZIF-94 (hydrophilic MOF) should make a big difference in how well the TFN membranes separate gases as ZIF-94 can attach and diffuse more CO_2 molecules than ZIF-8 because of the CO_2-philicity and hydrophilicity nature, that enhance its interaction with CO_2 molecules. For example, at normal conditions, ZIF-8 adsorbs about 0.7 mmol/g of CO_2 (Gadipelli et al., 2014; Liu et al., 2014), while ZIF-94 around 2.4–2.9 mmol/g of CO_2 (Cacho-Bailo et al., 2017). As a result, the TFN membranes made with 10 wt% ZIF-94(SALE) and ZIF-94 showed the best separation performance. The TFN/ZIF-94 membrane achieved a CO_2/CH_4 selectivity of 32.6 with a CO_2 permeance of 102 GPU, while the TFN/ZIF-94(SALE) membrane reached a selectivity of 40.0 with the same CO_2 permeance of 102 GPU.

The higher CO_2 permeance in TFN-ZIF-94 compared to TFN-ZIF94 (SALE) is likely due to differences in MOF particle size (larger particle size for ZIF-94 that for ZIF-94(SALE). Larger particles in TFN-ZIF-94 may create additional free volume and facilitate a greater gas transport compared to the smaller particles in TFN-ZIF94(SALE), which can lead to lower separation selectivities due to stronger aggregation generating zones in the TFN membrane in which not all the filler particles become surrounded by polymer. In any event, there may be a compromise between the gain in separation performance and the suitability of nanoparticles to constitute processable TFN membranes.

Fig. 8 plots the CO_2/CH_4 separation selectivity as a function of the CO_2 permeance, similar to Robeson plots used for comparing different

Table 4
CO_2/CH_4 mixture separation performance at 35 °C for TFN membranes with different loadings (5 −15 wt%) of ZIF-94(SALE) and ZIF-94 fillers.

Membrane	Permeance CO_2 (GPU)	Permeance CH_4 (GPU)	Selectivity (CO_2/CH_4)
TFN/ZIF−94(SALE) (5 %)	125 ± 1	4.6 ± 0.1	27.0 ± 0.1
TFN/ZIF−94(SALE) (10 %)	102 ± 7	3.7 ± 0.2	32.6 ± 1.9
TFN/ZIF−94(SALE) (15 %)	63 ± 6	2.4 ± 0.2	26.1 ± 0.8
TFN/ZIF−94 (5 %)	121 ± 6	5.1 ± 0.3	24.0 ± 0.6
TFN/ZIF−94 (10 %)	102 ± 15	2.7 ± 0.7	40.0 ± 4.8
TFN/ZIF−94 (15 %)	114 ± 2	4.1 ± 0.1	28.2 ± 0.4

membrane performances in gas separation (Robeson, 1991, 2008). Our tested membranes are contrasted with other Pebax® based membranes from literature (Guo et al., 2022; Martínez-Izquierdo et al., 2024; Wang et al., 2020; Xiang et al., 2017; Zhang et al., 2019). The TFN membranes in our study exhibit a high gas separation performance, equated to those reported with other Pebax® codes. It is noteworthy that this specific Pebax® Rnew® 30R51, unlike Pebax® 1657, has not been extensively studied for CO_2/CH_4 separation, especially as a thin composite membrane, besides having a 41 % of renewable carbon (measured by ASTM D6866 as reported by Arkema in the corresponding data sheet). Overall, Fig. 8 illustrates that incorporating both Pebax® Rnew® 30R51 thin layers and various ZIF particles on top of a PSF support (with a PTSMP gutter layer in between) enhances the gas separation performance, increasing the CO_2 permeance without compromising the CO_2/CH_4 selectivity. Furthermore, the performance of the fabricated membranes were not only compared with other Pebax® TFN membranes but also with different types of TFN membranes reported in the literature for CO_2/CH_4 separation (Cai et al., 2021; Yang et al., 2021). Fig. 8 shows that our results are within the range of other published data, further demonstrating the competitiveness of our membranes in terms of CO_2 permeance and CO_2/CH_4 selectivity.

4. Conclusions

This study demonstrates that by increasing the Pebax® Rnew® 30R51 concentration (0.25–5 wt%) in the casting solution used to spin coat the TFC membranes the CO_2 permeance decreases while enhancing the CO_2/CH_4 separation selectivity. The higher Pebax® concentration caused a thicker selective skin layer on the PSF support, favoring the selective interactions between CO_2 molecules and the functional groups within the Pebax®. However, beyond 2 wt%, the CO_2/CH_4 selectivity declines due to the potential Pebax aggregation or phase separation on the PSF surface. The temperature significantly influenced the TFC membrane performance, the higher temperatures increase polymer chain flexibility, leading to higher permeance for both CO_2 and CH_4 but reduced the CO_2/CH_4 selectivity, the latter due to the weakened interactions between CO_2 molecules and the Pebax® Rnew® 30R51.

The CO_2/CH_4 separation performance of TFN membranes is impacted by the addition of ZIF nanoparticles (ZIF-8, NH_2-ZIF-8 and ZIF-94) at varying loadings (5–15 wt%). A gradual increase in CO_2 permeance with higher ZIF loading suggests facilitated diffusion pathways. However, a significant reduction in CO_2/CH_4 selectivity occurs after reaching a certain ZIF loading (5 wt%), likely due to particle agglomeration within the Pebax® Rnew® 30R51 matrix. Moreover, the NH_2-ZIF-8 incorporation slightly enhances the CO_2/CH_4 separation selectivity compared to ZIF-8, probably due to specific interactions between amino groups of NH_2-ZIF-8 and CO_2 molecules favoring the CO_2 separation. Also, ZIF-94 exhibits a superior CO_2 affinity compared to ZIF-8 due to its hydrophilic nature, leading to higher CO_2/CH_4 selectivity. With the addition of ZIFs at 5 wt% loadings of ZIF-8, NH_2-ZIF-8, ZIF-94 (SALE) and ZIF-94, the CO_2 permeance increased (from 66 GPU for membrane TFC (2 %)) to 148, 99, 125 and 121, respectively. However, the CO_2/CH_4 separation selectivity decreased (from 37.5 GPU for membrane TFC (2 %)) to 29.4, 37.0, 27.0 and 24.0, respectively.

Overall, the fabricated TFN membranes exhibited high gas separation performances comparable to those of the literature-reported Pebax® based membranes, highlighting the potential of ZIF/ Pebax® Rnew® 30R51 composites to enhance the gas separation efficiency. Finally, these membranes hold promise for reducing greenhouse gas emissions and improving natural gas processing efficiency, addressing environmental and energy challenges. Further research on optimizing the fabrication and scaling up production could enable widespread industrial applications, supporting the sustainability goals and energy needs.

CRediT authorship contribution statement

Mohamed Yahia: Writing – review & editing, Writing – original draft, Visualization, Supervision, Methodology, Formal analysis. **Dalia Refaat:** Writing – review & editing, Writing – original draft, Visualization, Validation, Methodology, Investigation, Data curation, Conceptualization. **Joaquin Coronas:** Writing – review & editing, Writing – original draft, Resources, Project administration, Methodology, Funding acquisition, Conceptualization.

Declaration of Competing Interest

The authors declare that they have no known competing financial interests or personal relationships that could have appeared to influence the work reported in this paper.

Acknowledgements

This work acknowledges grants PID2022–138582OB-I00 (funded by MCIN/AEI/10.13039/501100011033/ and by “ERDF A way of making Europe”), TED2021–130621B-C4 (funded by MCIN/AEI/10.13039/501100011033/ and by and the European Union-NextGeneration EU) and CEX2023–001286-S (funded by MICIU/AEI /10.13039/501100011033). M. Yahia was supported through “the María Zambrano program” funded by both “the European Union’s Next-Generation-EU” and “the Spanish Ministerio de Universidades”. Financial assistance from the Government of Aragón (T68_23R) is also acknowledged. Technical guidance and instrumentation provided by “the Universidad de Zaragoza” through “the national facility ELECMI ICTS Laboratorio de Microscopías Avanzadas” and “the Servicio General de Apoyo a la Investigación-SAI” are thanked.

Appendix A. Supporting information

Supplementary data associated with this article can be found in the online version at doi:10.1016/j.psep.2024.10.053.

References

Aguado, S., Canivet, J., Farrusseng, D., 2010. Facile shaping of an imidazolate-based MOF on ceramic beads for adsorption and catalytic applications. Chem. Commun. 46, 7999–8001.
Alkandari, S.H., Castro-Dominguez, B., 2024. Advanced and sustainable manufacturing methods of polymer-based membranes for gas separation: a review. Front. Membr. Sci. Technol. 3, 1390599.
Baker, R.W., Low, B.T., 2014. Gas separation membrane materials: a perspective. Macromolecules 47, 6999–7013.
Basu, S., Khan, A.L., Cano-Odena, A., Liu, C., Vankelecom, I.F., 2010. Membrane-based technologies for biogas separations. Chem. Soc. Rev. 39, 750–768.
Berned-Samatán, V., Téllez, C., Coronas, J., 2023. Double-Layered Pebax® 3533/ZIF-8 membranes with single-walled carbon nanotube buckypapers as support for gas separation. Membranes 71.
Biruh, S., Hilmi, M., 2012. Natural gas purification technologies - major advances for CO2 separation and future directions. In: Hamid, A.A.-M. (Ed.), Advances in Natural Gas Technology. IntechOpen, Rijeka, p. Ch. 9.
Cacho-Bailo, F., Etxeberría-Benavides, M., Karvan, O., Téllez, C., Coronas, J., 2017. Sequential amine functionalization inducing structural transition in an aldehyde-containing zeolitic imidazolate framework: application to gas separation membranes. CrystEngComm 19, 1545–1554.
Cai, X., Yuan, Y., Sheng, M., Wang, J., Wang, Z., 2021. High-performance CO2/CH4 separation membrane fabrication with PVAm modified by the MOFs containing amine groups. J. Nat. Gas. Sci. Eng. 89, 103874.
Dai, Y., Ruan, X., Yan, Z., Yang, K., Yu, M., Li, H., Zhao, W., He, G., 2016. Imidazole functionalized graphene oxide/PEBAX mixed matrix membranes for efficient CO_2 capture. Sep. Purif. Technol. 166, 171–180.
Dong, G., Li, H., Chen, V., 2013. Challenges and opportunities for mixed-matrix membranes for gas separation. J. Mater. Chem. A 1, 4610–4630.
Embaye, A.S., Martínez-Izquierdo, L., Malankowska, M., Téllez, C., Coronas, J., 2021. Poly(ether-block-amide) copolymer membranes in CO_2 separation applications. Energy Fuels 35, 17085–17102.
Freeman, B.D., 1999. Basis of permeability/selectivity tradeoff relations in polymeric gas separation membranes. Macromolecules 32, 375–380.

Gadipelli, S., Travis, W., Zhou, W., Guo, Z., 2014. A thermally derived and optimized structure from ZIF-8 with giant enhancement in CO_2 uptake. Energy Environ. Sci. 7, 2232–2238.
Guo, H., Wei, J., Ma, Y., Deng, J., Yi, S., Wang, B., Deng, L., Jiang, X., Dai, Z., 2022. Facilitated transport membranes for CO_2/CH_4 separation State of the art. Adv. Membr. 2, 100040.
Gupta, K.M., Qiao, Z., Zhang, K., Jiang, J., Interfaces, 2016. Seawater pervaporation through zeolitic imidazolate framework membranes: atomistic simulation study. ACS Appl. Mater. Interfaces 8, 13392–13399.
Hasan, M.R., Paseta, L., Malankowska, M., Téllez, C., Coronas, J., 2022. Synthesis of ZIF-94 from recycled mother liquors: study of the influence of its loading on postcombustion CO_2 capture with Pebax based mixed matrix membranes. Adv. Sustain. Syst. 6, 2100317.
Hou, W., Cheng, J., Liu, N., Yang, C., Chen, Y., Zhang, H., Ye, B., Zhou, J., 2022. Selection-diffusion-selection mechanisms in ordered hierarchically-porous MOF-on-MOF: ZIF-8 @NH2-MIL-125 for efficient CO_2 separation. J. Environ. Chem. Eng. 10, 108029.
Jomekian, A., Behbahani, R.M., Mohammadi, T., Kargari, A., 2016. CO_2/CH_4 separation by high performance co-casted ZIF-8/Pebax 1657/PES mixed matrix membrane. J. Nat. Gas. Sci. Eng. 31, 562–574.
Kárászová, M., Zach, B., Petrusová, Z., Červenka, V., Bobák, M., Šyc, M., Izák, P., 2020. Post-combustion carbon capture by membrane separation, review. Sep. Purif. Technol. 238, 116448.
Kattula, M., Ponnuru, K., Zhu, L., Jia, W., Lin, H., Furlani, E.P., 2015. Designing ultrathin film composite membranes: the impact of a gutter layer. Sci. Rep. 5, 15016.
Li, T., Pan, Y., Peinemann, K.-V., Lai, Z., 2013. Carbon dioxide selective mixed matrix composite membrane containing ZIF-7 nano-fillers. J. Membr. Sci. 425-426, 235–242.
Liu, D., Gu, J., Liu, Q., Tan, Y., Li, Z., Zhang, W., Su, Y., Li, W., Cui, A., Gu, C., 2014. Metal-organic frameworks reactivate deceased diatoms to be efficient CO_2 absorbents. Adv. Mater. 26, 1229–1234.
Lu, P., Liang, S., Zhou, T., Mei, X., Zhang, Y., Zhang, C., Umar, A., Wang, Q., 2016. Layered double hydroxide/graphene oxide hybrid incorporated polysulfone substrate for thin-film nanocomposite forward osmosis membranes. RSC Adv. 6, 56599–56609.
Luo, W., Hou, D., Guan, P., Li, F., Wang, C., Li, H., Zhang, X., Huang, G., Lu, X., Li, Y., Zhou, T., 2024. Pebax membranes-based on different two-dimensional materials for CO2 capture: a review. Sep. Purif. Technol. 340, 126744.
Madhav, D., Malankowska, M., Coronas, J., 2020. Synthesis of nanoparticles of zeolitic imidazolate framework ZIF-94 using inorganic deprotonators. N. J. Chem. 44, 20449–20457.
Martínez-Izquierdo, L., Malankowska, M., Sánchez-Laínez, J., Téllez, C., Coronas, J., 2019. Poly(ether-block-amide) copolymer membrane for CO_2/N_2 separation: the influence of the casting solution concentration on its morphology, thermal properties and gas separation performance. R. Soc. Open Sci. 6, 190866.
Martínez-Izquierdo, L., Malankowska, M., Téllez, C., Coronas, J., 2021. Phase inversion method for the preparation of Pebax® 3533 thin film membranes for CO_2/N_2 separation. J. Environ. Chem. Eng. 9, 105624.
Martínez-Izquierdo, L., Téllez, C., Coronas, J., 2022b. Highly stable Pebax® Renew® thin-film nanocomposite membranes with metal organic framework ZIF-94 and ionic liquid [Bmim][BF_4] for CO_2 capture. J. Mater. Chem. A 10, 18822–18833.
Martínez-Izquierdo, L., Perea-Cachero, A., Malankowska, M., Téllez, C., Coronas, J., 2022a. A comparative study between single gas and mixed gas permeation of polyether-block-amide type copolymer membranes. J. Environ. Chem. Eng. 10, 108324.
Martínez-Izquierdo, L., García-Comas, C., Dai, S., Navarro, M., Tissot, A., Serre, C., Téllez, C., Coronas, J., 2024. Ultrasmall functionalized UiO-66 nanoparticle/polymer Pebax 1657 thin-film nanocomposite membranes for optimal CO_2 separation. ACS Appl. Mater. Interfaces 16, 4024–4034.
Morris, W., He, N., Ray, K.G., Klonowski, P., Furukawa, H., Daniels, I.N., Houndonougbo, Y.A., Asta, M., Yaghi, O.M., Laird, B.B., 2012. A combined experimental-computational study on the effect of topology on carbon dioxide adsorption in zeolitic imidazolate frameworks. J. Phys. Chem. C 116, 24084–24090.
Murali, R.S., Jha, A., Aarti, Divekar, S., Dasgupta, S., 2023a. Synthesis and characterization of a high-performance bio-based Pebax membrane for gas separation applications. Mater. Adv. 4, 4843–4851.
Murali, R.S., Jha, A., Aarti, Divekar, S., Dasgupta, S.J.M.A., 2023b. Synthesis and Characterization of High Performance Bio-based Pebax Membrane for Gas Separation Applications.
Nguyen, L.T., Ky, K.L., Nam, T., 2012. A zeolite imidazolate framework ZIF-8 catalyst for friedel-crafts acylation. Chin. J. Catal. 33, 688–696.
Park, K.S., Ni, Z., Côté, A.P., Choi, J.Y., Huang, R., Uribe-Romo, F.J., Chae, H.K., O'Keeffe, M., Yaghi, O.M., 2006. Exceptional chemical and thermal stability of zeolitic imidazolate frameworks. Proc. Natl. Acad. Sci. 103, 10186–10191.
Rabiee, H., Ghadimi, A., Mohammadi, T., 2015. Gas transport properties of reverse-selective poly(ether-b-amide6)/[Emim][BF4] gel membranes for CO2/light gases separation. J. Membr. Sci. 476, 286–302.
Rafiul Hasan, M., Moriones, A., Malankowska, M., Coronas, J., 2023. Study on the recycling of zeolitic imidazolate frameworks and polymer Pebax® 1657 from their mixed matrix membranes applied to CO_2 capture. Sep. Purif. Technol. 304, 122355.
Robeson, L.M., 1991. Correlation of separation factor versus permeability for polymeric membranes. J. Membr. Sci. 62, 165–185.
Robeson, L.M., 2008. The upper bound revisited. J. Membr. Sci. 320, 390–400.
Saini, N., Awasthi, K., 2022. Insights into the progress of polymeric nano-composite membranes for hydrogen separation and purification in the direction of sustainable energy resources. Sep. Purif. Technol. 282, 120029.
Sánchez-Laínez, J., Zornoza, B., Téllez, C., Coronas, J., 2018. Asymmetric polybenzimidazole membranes with thin selective skin layer containing ZIF-8 for H2/CO2 separation at pre-combustion capture conditions. J. Membr. Sci. 563, 427–434.
Tanvidkar, P., Appari, S., Kuncharam, B.V.R., 2022. A review of techniques to improve performance of metal organic framework (MOF) based mixed matrix membranes for CO2/CH4 separation. Rev. Environ. Sci. Bio/technol. 21, 539–569.
Tena, A., Shishatskiy, S., Filiz, V., 2015. Poly(ether–amide) vs. poly(ether–imide) copolymers for post-combustion membrane separation processes. RSC Adv. 5, 22310–22318.
Thompson, J.A., Blad, C.R., Brunelli, N.A., Lydon, M.E., Lively, R.P., Jones, C.W., Nair, S., 2012. Hybrid zeolitic imidazolate frameworks: controlling framework porosity and functionality by mixed-linker synthesis. Chem. Mater. 24, 1930–1936.
Thompson, J.A., Brunelli, N.A., Lively, R.P., Johnson, J.R., Jones, C.W., Nair, S., 2013. Tunable CO_2 adsorbents by mixed-linker synthesis and postsynthetic modification of zeolitic imidazolate frameworks. J. Phys. Chem. C 117, 8198–8207.
Wang, M., Quan, K., Zheng, X., Cao, Y., Cui, X., Xue, M., Pan, F., 2020. Facilitated transport membranes by incorporating self-exfoliated covalent organic nanosheets for CO_2/CH_4 separation. Sep. Purif. Technol. 237, 116457.
Wang, S., Li, X., Wu, H., Tian, Z., Xin, Q., He, G., Peng, D., Chen, S., Yin, Y., Jiang, Z., 2016. Advances in high permeability polymer-based membrane materials for CO_2 separations. Energy Environ. Sci. 9, 1863–1890.
Wang, X., Zhang, Y., Chen, X., Wang, Y., He, M., Shan, Y., Li, Y., Zhang, F., Chen, X., Kita, H., 2022. Preparation of Pebax 1657/MAF-7 mixed matrix membranes with enhanced CO_2/N_2 separation by active site of triazole ligand. Membranes 12, 786.
Wang, Y., Li, H., Dong, G., Scholes, C., Chen, V., 2015. Effect of fabrication and operation conditions on CO_2 separation performance of PEO–PA block copolymer membranes. Ind. Eng. Chem. Res. 54, 7273–7283.
Xiang, L., Pan, Y., Jiang, J., Chen, Y., Chen, J., Zhang, L., Wang, C., 2017. Thin poly (ether-block-amide)/attapulgite composite membranes with improved CO_2 permeance and selectivity for CO_2/N_2 and CO_2/CH_4. Chem. Eng. Sci. 160, 236–244.
Xiong, Y., Deng, N., Wu, X., Zhang, Q., Liu, S., Sun, G., 2022. De novo synthesis of amino-functionalized ZIF-8 nanoparticles: enhanced interfacial compatibility and pervaporation performance in mixed matrix membranes applying for ethanol dehydration. Sep. Purif. Technol. 285, 120321.
Yahia, M., Phan Le, Q.N., Ismail, N., Essalhi, M., Sundman, O., Rahimpour, A., Dal-Cin, M.M., Tavajohi, N., 2021. Effect of incorporating different ZIF-8 crystal sizes in the polymer of intrinsic microporosity, PIM-1, for CO_2/CH_4 separation. Microporous Mesoporous Mater. 312, 110761.
Yahia, M., Lozano, L.A., Zamaro, J.M., Téllez, C., Coronas, J., 2024. Microwave-assisted synthesis of metal–organic frameworks UiO-66 and MOF-808 for enhanced CO_2/CH_4 separation in PIM-1 mixed matrix membranes. Sep. Purif. Technol. 330, 125558.
Yang, L., Yang, H., Wu, H., Zhang, L., Ma, H., Liu, Y., Wu, Y., Ren, Y., Wu, X., Jiang, Z., 2021. COF membranes with uniform and exchangeable facilitated transport carriers for efficient carbon capture. J. Mater. Chem. A 9, 12636–12643.
Yu, S., Li, C., Zhao, S., Chai, M., Hou, J., Lin, R., 2024. Recent advances in the interfacial engineering of MOF-based mixed matrix membranes for gas separation. Nanoscale.
Zhang, J., Xin, Q., Li, X., Yun, M., Xu, R., Wang, S., Li, Y., Lin, L., Ding, X., Ye, H., Zhang, Y., 2019. Mixed matrix membranes comprising aminosilane-functionalized graphene oxide for enhanced CO_2 separation. J. Membr. Sci. 570-571, 343–354.
Zhang, Y., Sunarso, J., Liu, S., Wang, R., 2013. Current status and development of membranes for CO2/CH4 separation: a review. Int. J. Greenh. Gas. Control 12, 84–107.
Zou, X., Zhu, G., 2018. Microporous organic materials for membrane-based gas separation. Adv. Mater. 30, 1700750.